International Journal of Nanoelectronics and Materials

In Press, Accepted Manuscript – Note to user

Microstructures, Absorption Spectra, and Magnetic Properties of Core-shell Fe_3O_4@Ag Nanoparticles for Enhancing Sensitivity of Surface Plasmon Resonance (SPR) Sensor

Juharni[1], Ilyas Maulana Yahya[1], Edi Suharyadi[1,*], Takeshi Kato[2,3], and Satoshi Iwata[3]

[1]Department of Physics, Universitas Gadjah Mada, Yogyakarta, Indonesia
[2]Department of Electronics, Nagoya University, Japan
[3]Institute of Materials and System for Sustainability, Nagoya University, Japan

Received 17 August 2020, Revised 30 November 2020, Accepted 30 January 2021

ABSTRACT

The purpose of this study is to enhance the sensitivity of Surface Plasmon Resonance (SPR) sensor using core-shell Fe_3O_4@Ag nanoparticles (NPs). Fe_3O_4@Ag NPs were synthesized by co-precipitation method with various concentration of Ag as a shell. The crsytal structure of Fe_3O_4 corresponds to the cubic inverse spinel structure. The particle size of Fe_3O_4@Ag NPs with Ag concentration of 40mM is 13.8 nm. The saturation magnetization (Ms), and coercivity field (Hc) of Fe_3O_4@Ag NPs with Ag concentration of 20mM is 52.9 emu/g and 157.2 Oe, respectively, and then decreased with the increase of Ag concentration. An intensity of absorption peak increased with the increase of Ag concentration. A spherical nanoparticle consisting of a spherical Fe_3O_4 core covered by an Ag shell, was used as an active material to increase the signal detection of SPR, with a wavelength of 632.8 nm in the Kretschmann configuration. The system consists of a three-layer materials, i.e., prism/Au/Fe_3O_4@Ag NPs. The results show that the SPR angle shifted to the larger angle of incident light by using Fe_3O_4@Ag NPs and the addition of a core-shell in the conventional SPR-based biosensor leads to the enhancement of the SPR biosensor sensitivity.

Keywords: core-shell, Fe_3O_4@Ag, sensitivity, Surface Plasmon Resonance (SPR).

1. INTRODUCTION

The surface plasmon resonance (SPR) biosensor has become a crucial optical biosensing for rapid and ultra-sensitive detection of biological analytes, with applications in medical diagnostic, environmental monitoring, agriculture, and for food quality and safety [1,2]. For example, in medical diagnostic, it used to be rapid detection of covid-19 [3] and etoposide detection [4]. Moreover, the presences of germs and environmental pollution demands a quick and appropriate measurement to give information about the food safety and quality for food industry and control authorities, thus, SPR is used for bacteria detection, pathogen detection, formalin detection [5]. Compared with other biosensors, SPR biosensors enable real-time monitoring of the binding of target bacteria with less reagent consumption [6].

This detection techniques depend on the interaction of the light and nanostructured materials. The surface plasmon resonance (SPR) phenomenon is a variation of the incident wave angle in which the wave reflectance is observed as a function of the incident angle. The active material to generate surface plasmon polariton (SPP) is used in gold and silver metals and the material detected used is a biomolecular-based dielectric material consisting of biorecognition and analyte elements. The approach is known to have produced a highly sensitive phenomenon [7,8].

The system of SPR works according to the changes of refractive index of the material and depends on the refractive index of the prism, dielectric constant of metal, index of refraction of the object or material detected, and wavelength of incident light. The advantages of SPR is fast response detection, real-time detection, and label-free technique [9,10].

*corresponding author: esuharyadi@ugm.ac.id

The weakness of conventional SPR is limited in their ability to resolve complex sample, extremely dilute concentration, or small molecular weight [11, 12]. To solve this limitation, researchers have worked about development of SPR sensitivity by using Fe_3O_4 magnetic nanoparticles [13, 14]. The use of Fe_3O_4 nanoparticles increases the ability of SPR to bind biological material in nanometer scale or low concentration [15], because Fe_3O_4 NPs has a large surface to interact with biomolecules and has a high absorption [13].

The results confirm that Fe_3O_4 NPs can be used as a powerful amplification agent to provide a sensitive approach to detect adenosine by SPR within the range of 10−10 000 nM, which is much superior to the detection result obtained by a general SPR sensor [14]. However, a direct contact between Fe_3O_4 NPs and biomolecules can make a damage of surface of Fe_3O_4 NPs. Besides that, it will be easier to occur aggregation and oxidation that can eliminate the magnetic properties of Fe_3O_4 NPs [16].

Covering Fe_3O_4 NPs with Ag NPs is a solution not only to decrease aggregation and oxidation, but also to generate of plasmon, thus the sensitivity of SPR biosensor will enhance. Besides, using Ag NPs is also to emphasize on heavy metallic ion detection [17]. In this work, microstructures, magnetic properties, and absorption spectra of core-shell Fe_3O_4@Ag nanoparticles is investigated. The plasmonic phenomena of core-shell Fe_3O_4@Ag nanoparticles with various Ag concentration is also studied.

2. MATERIALS AND METHODS

2.1. Reagents

All the reagents used for the synthesis NPs were pure analytical grade materials purchased from Merck (Darmstadt, GFR) and used without further purification. Iron III chlorite hexahydrate ($FeCl_3.6H_2O$), Ferrous sulfate heptahydrate ($FeSO_4.7H_2O$), (3-Aminopropyl)trimethoxysilane (APTMS) 97%, Silver Nitrate ($AgNo_3$), Ammonia Aqueous (NH_4OH) 25%, H_2O, and Ethanol (CH_3CH_2OH) 96%.

2.2. Synthesis of Fe_3O_4 nanoparticles

Fe_3O_4 NPs were firstly fabricated by using co-precipitation method. The 8.109 g of $FeCl_3.6H_2O$ and 4.170 g of $FeSO_4.7H_2O$ were mixed in 30 ml of H_2O and stirred at 450 rpm for 15 minutes. Furthemore, 60 ml of NH_4OH 10% (24 ml of NH_4OH and 36 ml H_2O) was added slowly into solution and treated at a temperature of 60 ^{0}C for 90 minutes. Thereafter, nanoparticles were magnetically separated by attaching external magnetic field, which were then washed several times with distilled water. The precipitated solution was dried using a furnace at temperature of 80 °C for 2 hours [18].

2.3. Synthesis of Fe_3O_4-APTMS nanoparticles

To link between Fe_3O_4 and Ag, APTMS is used as a linker. The 500 mg of Fe_3O_4 NPs, 10 ml of APTMS, 10 ml of NH_4OH 25% and 200 ml of CH_3CH_2OH were sonified for 1 hour at room temperature. Then, the mixture is washed three times and dry at 70 °C for 2 hours [19].

2.4. Synthesis of core-shell Fe_3O_4@Ag nanoparticles

Core-Shell Fe_3O_4@Ag MNPs were synthesized using the aqueous solution method. The 400 mg of Fe_3O_4 NPs-APTMS, $AgNO_3$ with various concentration of 20, 40, 60, 80, 100 mM, and 400 ml of CH_3CH_2O were mixed at room temperature for 4 hours. After the reaction, core-shell Fe_3O_4@Ag NPs is isolated from the mixture using a magnet permanent and furnace at 70 °C for 2 hours [20].

2.5. Characterization of core-shell Fe_3O_4@Ag nanoparticles

The core-shell Fe_3O_4@Ag nanoparticles would be characterized using X-ray Diffractometer (XRD), UV-Visible spectroscopy, Transmission Electron Microscopy (TEM) and Vibrating Sample Magnetometer (VSM). The SPR measurement, used a wavelength of 632.8 nm in the Kretschmann configuration. The method of nanoparticles deposition used spray method.

3. RESULTS AND DISCUSSION

3.1. Characterization of core-shell Fe_3O_4@Ag NPs

The XRD pattern of Fe_3O_4@Ag NPs is demonstrated by Figure 1. The formulation to calculate the crystallite size of NPs applied the Debye-Sherrer equation [21] :

$$D=k\lambda/\beta \cos\theta \quad (1)$$

where k = 0.95 is Sherrer's constant, λ is the X-ray wavelength, β is the full width at half maximum, and θ is the Bragg difraction angle. The position of peak at 30.1° (220), 35.5° (311), 43.1° (400), 53.4° (422), 57.1° (511), and 62.8° (440), corresponds to the cubic inverse spinel structure of the Fe_3O_4 (ICDD No. 88-0315). For Fe_3O_4, the peak indicates that stabilizers, Ag NPs, and linkers (APTMS) did not influence the magnetite crystal structure. The additional peak of X-ray diffraction patterns at angular positions 38.1° (111), 44.3° (200), and 64.4° (220), are assigned to metallic silver (Ag NPs) [20].

At the peak of the diffraction plane (311), the increase of Ag concentration caused shift in direction of a larger angle. An angle shift is caused by an increase in the distance between fields diffraction. Enlarge the distance between the fields tightly with magnification crystal lattice size. Meanwhile, the size of the crystal lattice depends on the nanoparticles the distribution patterns of Ag^+ and Fe^{3+} ions in the tetrahedral and octahedral spaces [22].

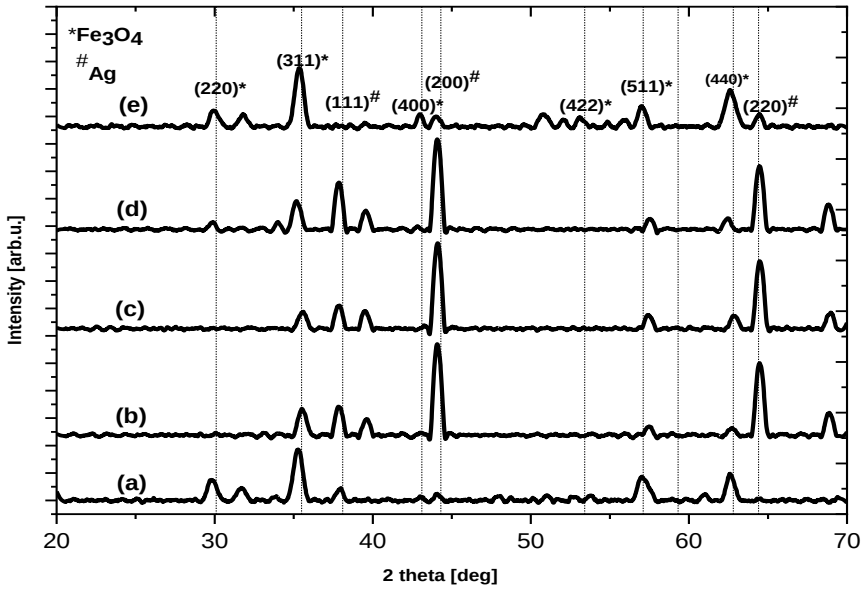

Figure 1. X-Ray patterns of core-shell Fe_3O_4@Ag NPs with various Ag concentration of (a) 20, (b) 40, (c) 60 (d) 80, and (e) 100 mM

Table 1. The crystallite size of core-shell Fe_3O_4@Ag nanoparticles

Ag concentration (mM)	crystallite size (nm)
20	12.2
40	13.1

60	13.4
80	13.3
100	12.1

Generally, the increase of Ag concentration up to 80 mM, the crystallite size of Fe_3O_4 NPs slightly increases, as shown in Table 1. It is a proof that Ag succesfully covered the magnetite materials. However, for 100 mM, the crystallite size slightly decreases. It indicates that the lack of Ag^+ ions occupy the octahedral sub space. From scherrer formula using the reflection planes (311), the lattice parameter *a* of Fe_3O_4@Ag NPs is also determined. The average of lattice paramater calculation is 8.4 nm.

Increasing the concentration of Ag caused the migration of Ag^+ ions to octahedral sub space. Similarly, Fe^{3+} ions undergo migration to sub octahedral space. The amount of Fe^{3+} ions occupying more octahedral sub space dominant than the tetrahedral sub space. As a result, the radius is average of sub space octahedral will be greater than tetrahedral sub space. Therefore, the size of the crystallite and the parameters of the dominant crystal lattice are determined by the average sub-octahedral finger radius [22].

The effect of Ag concentration on crystal size also has an important role during the nucleation and growth of crystallites. In the nucleation process will involve the process of absorption or desorption of ions to occupy certain sub spaces in the structure of the nanoparticle crystal structure. Fe_3O_4 nanoparticles are a complex system because it involves more than two ions in the nucleation process. The process of nucleation and growth of crystallite nanoparticles are influenced by the possibility of an ion occupying a certain sub space based on the level of affinity of the ion in the crystal field of each sub space. The size of the nanoparticles is more dominantly determined by the size of the ions occupying the octahedral sub space [23]. In this study, the assumption is the reduction in Ag concentration make the Ag^+ concentration in both crystal lattice sub chamber. Thus, it is also reduced, consequently the crystallite size will be smaller.

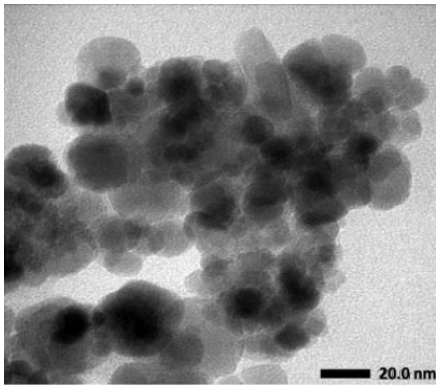

Figure 2. The TEM image of Fe_3O_4@Ag NPs 40 mM

The morphology, particle size and size distribution of core-shell Fe_3O_4@Ag 40 mM nanoparticles were recorded by TEM. The concentration of 40 mM was selected because it has a high intensity of the diffraction field. As given in Figure 2, the nanoparticle is not uniform and spherical in shape. The average of particle size is 13.8 nm. Their morphologies and size are strongly correlated with the preparation techniques.

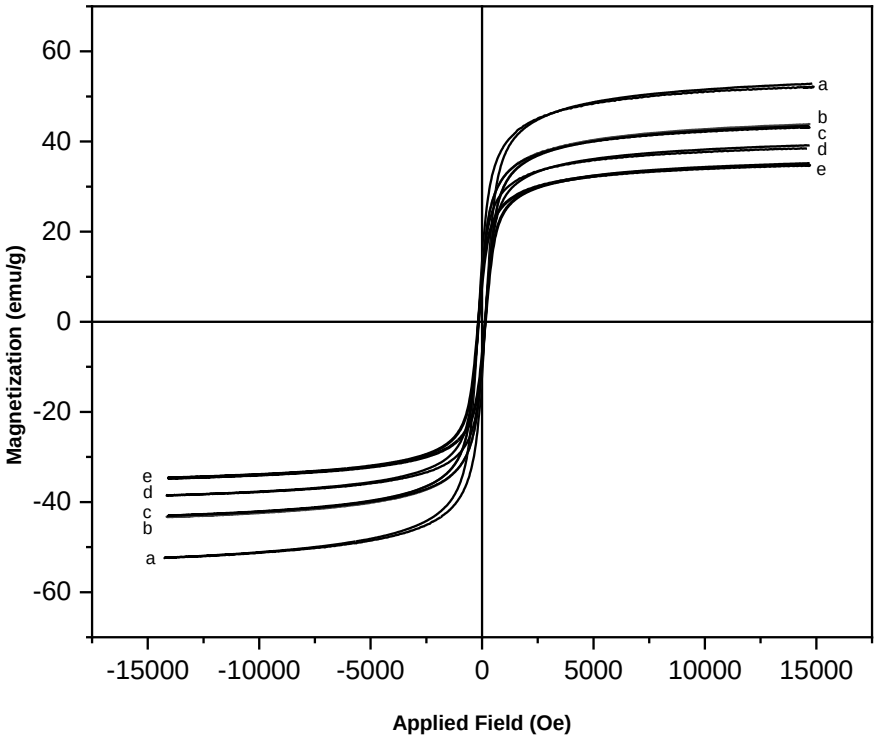

Figure 3. Magnetization versus applied magnetic field of core-shell Fe_3O_4@Ag NPs with various Ag concentration of (a) 20, (b) 40, (c) 60 (d) 80, and (e)100 mM

The magnetization curves of Fe_3O_4@Ag NPs are shown in Figure 3. The result show that Fe_3O_4@Ag NPs display soft ferromagnetic properties. Table 2 clearly describes that the increase of Ag concentration, the saturation magnetization (*Ms*) decreases [24].

Table 2. Magnetic properties of core-shell Fe_3O_4@Ag nanoparticles

Ag concentration (mM)	Remanent Magnetization (*Mr*)	Saturation Magnetization (*Ms*)	Coercivity Field (*Hc*)
20	12.8	52.9	157.2
40	10.3	43.9	153.3
60	10.4	43.5	155.4
80	9.7	39.2	150.5
100	8.3	35.1	149.7

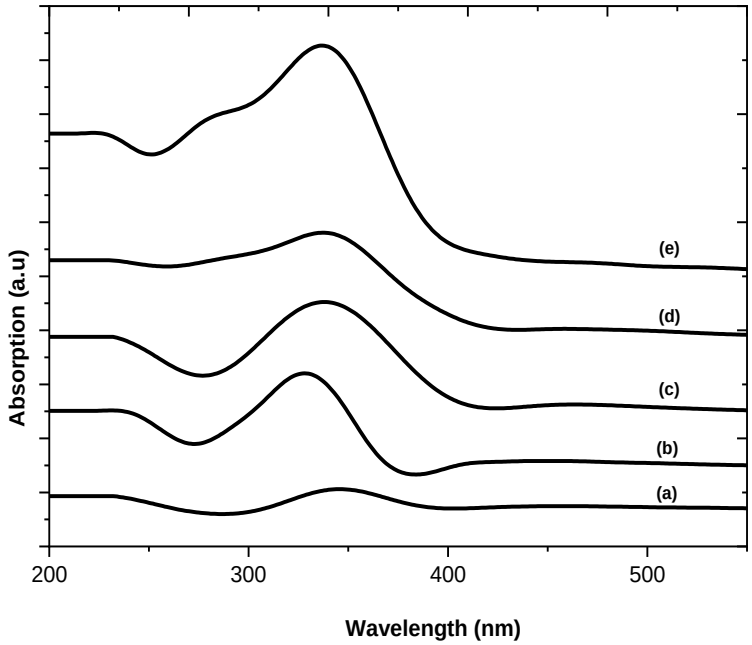

Figure 4. Spectrum of UV-Vis absorption of core-shell Fe_3O_4@Ag NPs with various Ag concentration of (a) 20, (b) 40, (c) 60 (d) 80, and (e)100 mM

Furthermore, the Fe_3O_4@Ag core-shell nanoparticle absorbance is studied UV-Visible Spectroscopy. This UV-Vis tool refers to absorption or reflectance spectroscopy in the spectral region that looks ultraviolet. In this electromagnetic spectrum region, atoms and molecules undergo electronic transitions. Therefore, absorption measures the transition from ground to excited state. The characterization of core-shell nanoparticles Fe_3O_4@Ag absorbance using UV-Visible Spectroscopy is presented in Figure 4. The results show that the absorption spectrum of the core-shell Fe_3O_4@Ag nanoparticles is at a wavelength of 328 - 338 nm. The wavelength range is characteristic of Ag nanoparticles. From these results, it can be concluded that Fe_3O_4 has been covered by Ag nanoparticles. Based on research previously, the characteristics of Ag are at 320 - 580 nm [25].

The minimum wavelength at 328 nm is the wavelength associated with the real and imaginary part of the dielectric constant of the Ag nanoparticles and this part is almost lost, so that, generally, the Ag plasmon band which is mostly found is at the peak of 426 nm. In addition, the figure also shows that the plasmon band is quite wide, accompanied by a long tail. This is related to the particle size distribution. The absorbance position is determined by several factors, such as the dielectric constant medium, size, dispersibility, defects, etc [25].

Nanoparticles	SPR angle of Prism/Au (Degree)	SPR angle of Prism/Au /nanoparticles (Degree)	The changes of SPR Angle (Degree)
Ag	42.78	42.81	0.03
Fe_3O_4	42.78	43.23	0.45
Fe_3O_4@Ag	42.78	48.56	5.78

Table 3. SPR angle of nanoparticles

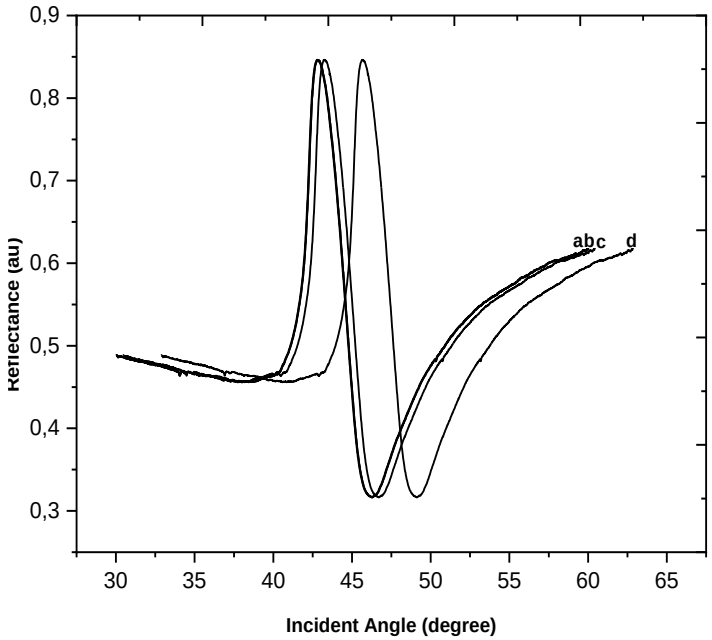

Figure 5. The SPR spectra of (a) Prism/Au (b) Prism/Au/Ag NPs (c) Prism/Au/Fe_3O_4 NPs, (d) Prism/Au/Fe_3O_4@Ag NPs

The SPR angle shifted from 0.03° to 0.45° after Prism/Au was deposited by Fe_3O_4 and Ag nanoparticles, as shown in Figure 5 and Table 3. However, using core-shell Fe_3O_4@Ag nanoparticles, the angle shifted more than using Fe_3O_4 and Ag. In general, the magnitude of the SPR depends on the prism refractive index, the dielectric constant of the metal, the wavelength of the incident ray, and the refractive index of the sample to be detected [26]. The SPR curve shift after deposition of Fe_3O_4, Ag, and core-shell Fe_3O_4@Ag nanoparticles is caused by a shift in the dispersion relation so that the meeting point between the SPP wave dispersion relation and the laser light wave dispersion relation have a shift. As a result, the SPR angle also changes. This SPR angle shift can be explained by shifting the wave dispersion relation at the time of resonance. The dielectric constant and the thickness of the Fe_3O_4, Ag, and core-shell Fe_3O_4@Ag layers affect the dispersion relation. The shift of the dispersion relation curve causes the coupling point between the light wave and the SP wave to change, thus the SPR angle changes [27].

Thus, core-shell construction in this study also has an important role in the SPR shift. In this study, core-shell which is a spherical nanoparticle and is composed of two parts, spherical nanoparticles as core (Fe_3O_4) which are covered by Ag nanoparticles as a shell. The advantage of Ag nanoparticles as a shell can increase the electromagnetic field around the surface of the material. Thus, it has the ability to strengthen the signal, and generate plasmon phenomena [28].

These core-shell nanoparticles have unique optical properties caused by their interaction with electromagnetic waves. This resonance occurs from the collective oscillations of conduction electrons in the metal (shell), which are coupled to electromagnetic fields and spread along the surface. At the plasmon resonance frequency, the cross-section of the core-shell absorption can be enlarged through variations in geometry Ag metal layer as a shell that surrounds the core (Fe_3O_4) will provide an optical response in the form of a spectrum associated with plasmon resonance on the inner and outer surface of the shell. Therefore, the SPR angle has a large shift if Ag covers Fe_3O_4. Besides, the shift is also caused by increasing dielectric constant from the combination of the two materials [29].

Based on the previous research, the dielectric constant owned by Fe_3O_4 nanoparticles and Ag nanoparticles is able to make the SPR angle shift towards a larger direction because the larger

mass and higher refractive index, so that the combination of the two materials in the form of core-shell Fe_3O_4@Ag will increase the dielectric constant value which causes the SPR angle shift much bigger [30]. Shifting angles toward larger angles is an indication that the sensitivity of the SPR is also increasing [31]. In this study, the combination of magnetic and plasmonic properties in the form of core-shell Fe_3O_4@Ag, in addition to being able to increase the SPR signal, the core-shell is also able to immobilize molecules in the SPR making, so it is easier to detect biomolecules with very small size and have low concentrations. In addition, the core-shell is biocompatible, capable of increasing binding with biomolecules as an analyte, reducing agglomeration, and resistance to corrosion. The use of Ag nanoparticles as a shell is because Ag uptake is greater than other precious metals. In certain studies, Ag nanoparticles are used to detect heavy metals such as Hg, Pb, etc [17].

In this research, using Ag nanoparticles on the surface of Fe_3O_4 in the core-shell Fe_3O_4@Ag nanoparticles could amplify the SPR sensor signal [30]. It is caused by the electromagnetic field of nanoparticles enhances the SPR signal due to the electronic coupling between the localized surface plasmon of nanoparticles and the surface plasmon of the gold film. The change of the real part of the refractive index with increased mass of the conjugate by nanoparticle deposition has contributed to the significant sensitivity enhancement of the sensor response [15]. Besides, Ag has the large ratio of the constants and exhibits ultrahigh sensitivity and the response [32, 33].

Moreover, the effect of core-shell Fe_3O_4@Ag nanoparticles in SPR biosensor by Kretschmann configuration with four layers shows that the angle of incident light shifted to the larger angle. Thus, if core-shell Fe_3O_4@Ag nanoparticles is applied to the SPR biosensor system, the changes lead to the increasing of SPR sensitivity. There are two types of coupling, coupled mode (low energy) at inner shell and anti-coupled mode (high energy) at outer shell. Therefore, the plasmon coupling is depend on the thickness of the metal shell [29]. Furthermore, the presence of Ag NPs protects Fe_3O_4 from agglomeration and oxidation. Ag Nps is also noble metallic that can generate plasmon for SPR phenomenon.

4. CONLUSION

Encapsulating Fe_3O_4 with Ag NPs demonstrates that the magnetization of Fe_3O_4 decrease with the increase of concetration . Based on the observation of SPR biosensor, the magnetic nanoparticles could be immobilized on the surface of SPR biosensor to get high signal detection by the shifting angle to the larger angle. After that, by using core-shell Fe_3O_4@Ag NPs also exhibit the incident angle of SPR shifted to larger angle more than Ag and Fe_3O_4 nanoparticles. By this measurement, it can be estimated that core-shell Fe_3O_4@Ag NPs can increase the sensitivity of SPR biosensor.

AKNOWLEDGEMENTS

This work was supported by the Education Fund Management Institute (LPDP) Indonesia; The grant of PTUPT No. 2873/UN1.DITLIT/DIT-LIT/PT/2020, Ministry of Research & Technology, Republic of Indonesia; and Nanof abrication Platform Consortium Project of Nagoya University, Minister of Culture, Sports, Science and Technology (MEXT) Nano-Project Platform, Japan.

REFERENCES

[1] Homola, J. Chem. Rev. 108 (2008) pp. 462 – 493.
[2] Guo, X. W. J. Biophoton. 5 (2012) pp. 483 – 501.
[3] Samson, R., Navale, G. R., and Dharne, M. S. Biotech. 10 (2020) pp. 385-1 – 9.
[4] Ozkan, A., Atar, N., and Yola, M. L. Biosens. Bioelectron. 130 (2019) pp. 293 – 298.
[5] Singh, S., Singh, P. K., Umar, A., Lohia, P., Albargi, H., Castañeda, L., and Dwivedi, D. K. Micromachines. 11 (2020) pp. 1 – 28.

[6] Shen, Y., Xu, L., and Li, Y. Compr Rev Food Sci Food. (2020) pp. 1 – 49.
[7] Endo, T., Yanagida, Y., and Hatsuzawa, T. Measurement. 41 (2008) pp. 1045 – 1053.
[8] Barizuddin, S., Bok, S., and Gangopadhyay, S. J. Nanomed Nanotechnol. 7 (2016) pp. 1000373-1 – 10.
[9] Homola, J. and Piliarik, M. Springer Ser Chem Sens Biosens. 4 (2006) pp. 45 – 67.
[10] Van De Donk, E., Zhang, X., and Simone, G. Biosens Bioelectron. 142 (2019) pp. 111514 – 111521.
[11] Soelberg, S. D., Stevens, R. C., Limaye, A. P., and Furlong, C. E. Anal. Chem. 81 (2009) pp. 2357 – 2363.
[12] Zeng, S., Baillargeat, D., Ho, H. P., and Yong, K. T. Chem. Soc. Rev. 43 (2014) pp. 3426 – 3452.
[13] Wang, J., Zhu, Z., Munir, A., and Zhou, H. S. Talanta. 84 (2011) pp. 783 – 788.
[14] Wang, J., Munir, A., Zhu, Z., and Zhou, H. S. Anal. Chem. 82 (2010) pp. 6782 – 6789.
[15] Tabasi, O. and Falamak, C. Anal. Methods. 10 (2018) pp. 1039 – 1059.
[16] Liang, R. P., Yao, G. H., Fan, L. X., and Qiu, J. D. Anal. Chim. Acta. 737 (2012) pp. 22 – 28.
[17] Amirjani, A. and Haghshenas, D. F. Sensors Actuat B-Chem. 273 (2018) pp. 1768 – 1779.
[18] Ekariyani, NY., Wardani, DP., Suharyadi, E., Daryono, BS., and Abraha, K. AIP Conf. Proc. 1755 (2016) pp. 155016-1 – 3.
[19] Du, J. and Jing, C. J. Phys. Chem. C. 115 (2011) pp. 17829 – 17835.
[20] Quynh, L. M., Dung, C. T., Mai, B. T., Huy H. V., Loc, N. Q., Hoa, N. Q., Thach, P. T., Anh, B. V., Thao, C. T., Nam, N. H., Nhung, H. T., Long, N. N., and Vu, L. V., J Immunoassay Immunochem 39 (2018) pp. 308 – 322.
[21] Sukirman, E. and Sarwanto, Y,. Jurnal Sains Materi Indonesia. 15 (2014) pp. 67 – 73.
[22] Rath, C., Anand, S., and Das, R. P. J. Appl. Phys. 91 (2001) pp. 2211 – 2215.
[23] Kareem, S. H., Ati, A. A., Shamsuddin, M., and Lee, S. L. Ceram. Int. 41 (2015) pp. 11702–11709.
[24] Mathew, D. S. and Juang, R. S. Chem. Eng. J. 129 (2007) pp. 51 – 65.
[25] Hamouda, R. A., Hussein, M. H., Abo-elmagd, R. A., and Bawazir, S. S. Sci. Rep. 9 (2019) pp. 13071-1 – 17.
[26] Homola, J., Yee, S. S., and Gauglitz, G. B. Chemical. 54 (1999) pp. 3 – 15.
[27] Supardianingsih, Suharyadi, E., and Abraha, K. In Proc. 5th International conference of Asian Union Magnetics Societies, Republic of Korea, (2018), G10-0312 p. 536.
[28] Lee, J. H., Cho, H. Y., Choi, H. K., Lee, J. Y., and Choi, J. W., Int. J. Mol. Sci. 19 (2018) pp. 2021-1 – 14.
[29] Widayanti, Abraha. K, and Utomo, A. B. S. Biosensors. 8 (2018) pp. 75 – 89.
[30] Wang, L., Sun, Y., Wang, J., Wang, J., Yu, A., Zhang, H., and Song, D. Colloids Surf B Biointerfaces. 84 (2011) pp. 484 – 490.
[31] Mahmudin, L., Ulum, M. S., Farhamsa, D., Suharyadi, E., Utomo, ABS., and Abraha, K. Journal of Physics: Conference Series, 1242 (2019) pp. 012027-1 – 5.
[32] Mitsushio, M., Miyashita, K., and Higo, M. Sens. Actuator A Phys 125 (2006) pp. 296 – 303.
[33] Chen, S. and Lin, C. Mater. Res. Express. 6 (2019) pp. 056503 – 056512.